

Supporting Information for

Ordered lithiophilic sites to regulate Li plating/stripping behavior for superior lithium metal anodes

By Bo Liu^a, Yan Zhang^a, Guoxiang Pan^b, Changzhi Ai^c, Shengjue Deng^a, Sufu Liu^a, Qi Liu^d,

Xiuli Wang^a, Xinhui Xia^{a*}, Jiangping Tu^{a*}

^a State Key Laboratory of Silicon Materials, Key Laboratory of Advanced Materials and Applications for Batteries of Zhejiang Province, and Department of Materials Science and Engineering, Zhejiang University, Hangzhou 310027, P. R. China

^b Department of Materials Chemistry, Huzhou University, Huzhou, 313000, P. R. China

^c State Key Laboratory of Marine Resource Utilization in South China Sea, Hainan University, Haikou 570228, P. R. China

^d Department of Physics, City University of Hong Kong, Kowloon, 999077, Hong Kong

E-mail address: helloxxh@zju.edu.cn (X. Xia); tujp@zju.edu.cn (J. Tu)

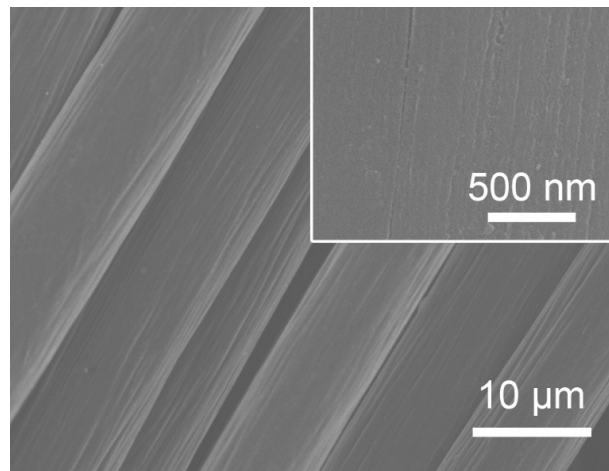


Fig. S1 SEM image of CC.

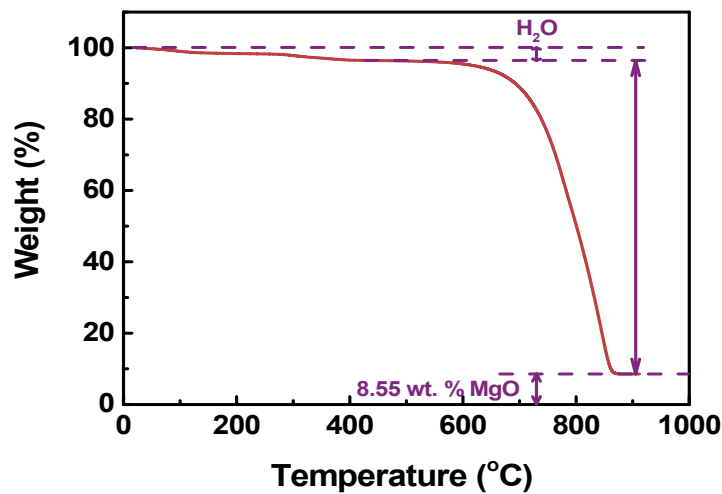


Fig. S2 TG curves of MgO/CC under air atmosphere.

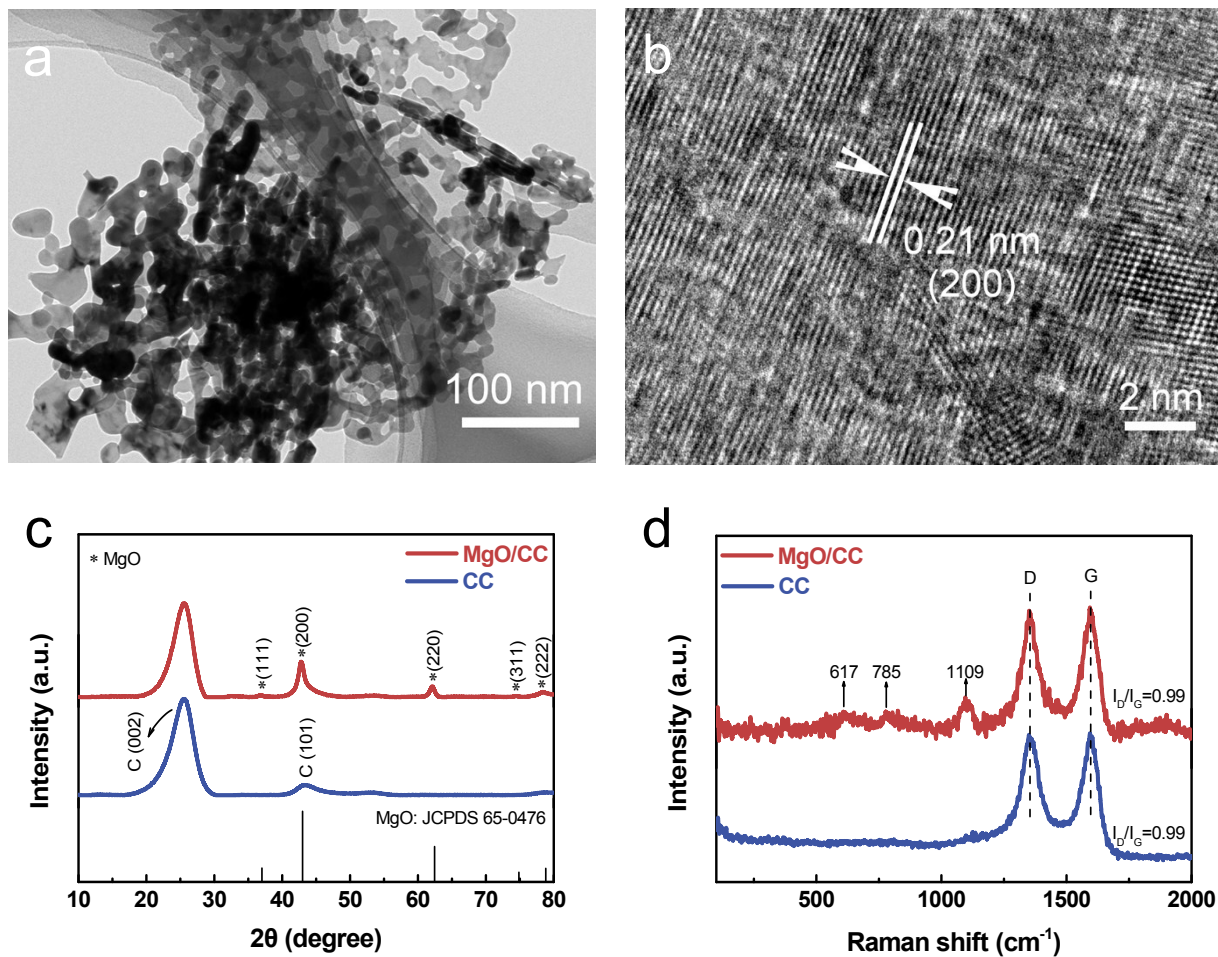


Fig. S3 (a) TEM and (b) HRTEM images of MgO/CC. (c) XRD patterns and d) Raman spectra of MgO/CC and CC.

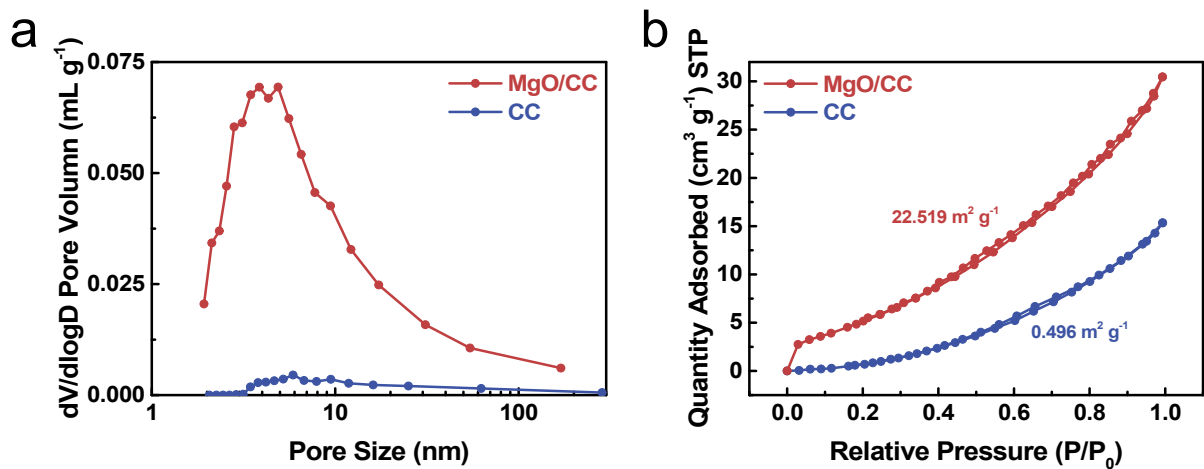


Fig. S4 (a) BET characterization and (b) N_2 adsorption–desorption isothermal analysis of MgO/CC and CC.

Table. S1. BET results of MgO/CC

Sample	Pore Area _{total} ($\text{m}^2 \text{ g}^{-1}$)	Pore Size _{average} (nm)	Pore Volume ($\text{cm}^3 \text{ g}^{-1}$)
MgO/CC	22.519	5.490	0.047
CC	0.496	9.181	0.003

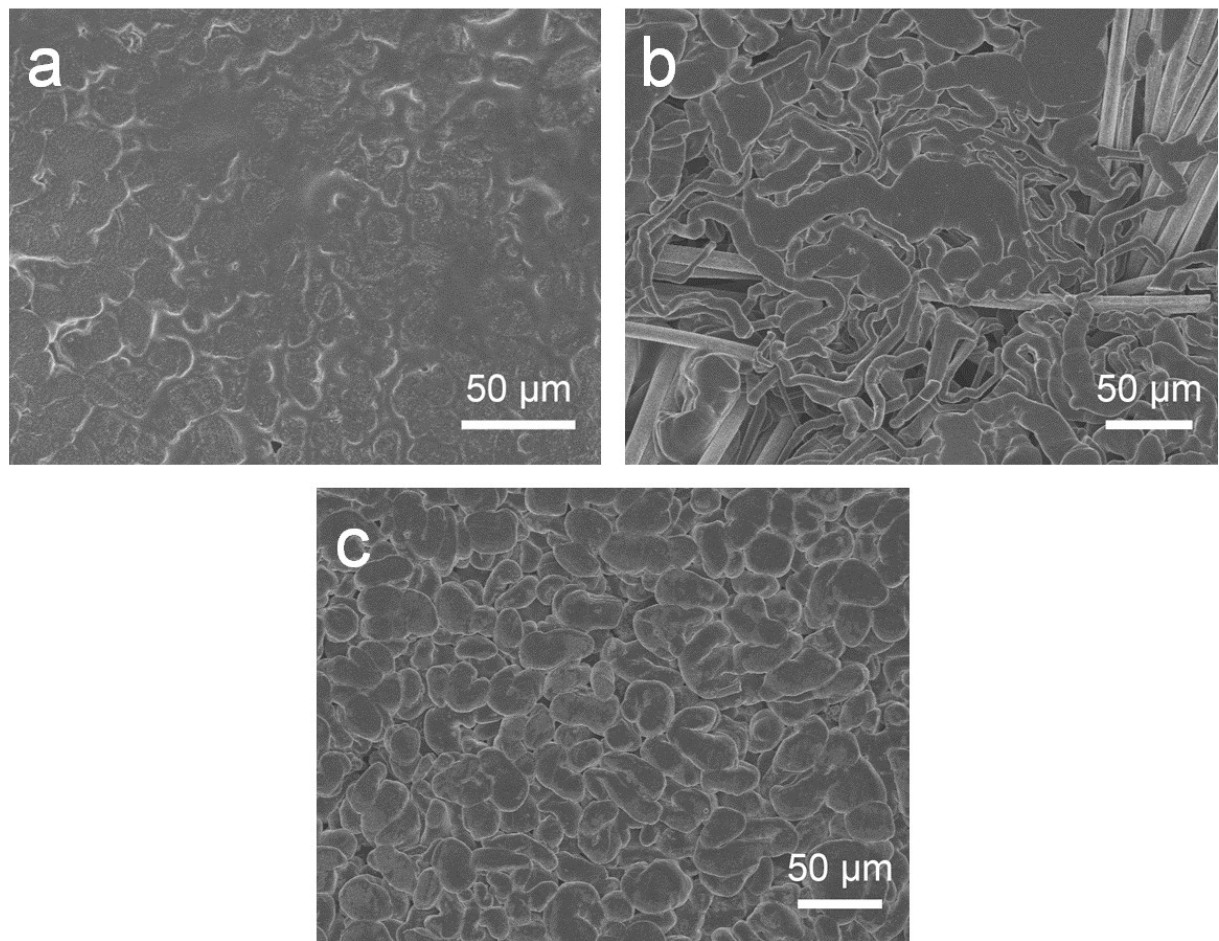


Fig. S5 SEM images of (a) MgO/CC, (b) CC and (c) Cu electrode after plating Li of 12 mA h

cm^{-2} .

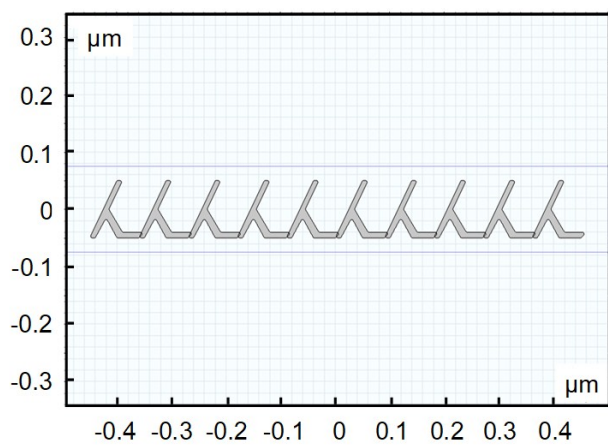


Fig. S6 Geometric construction of nanosheets in COMSOL Mutiphysics simulations.

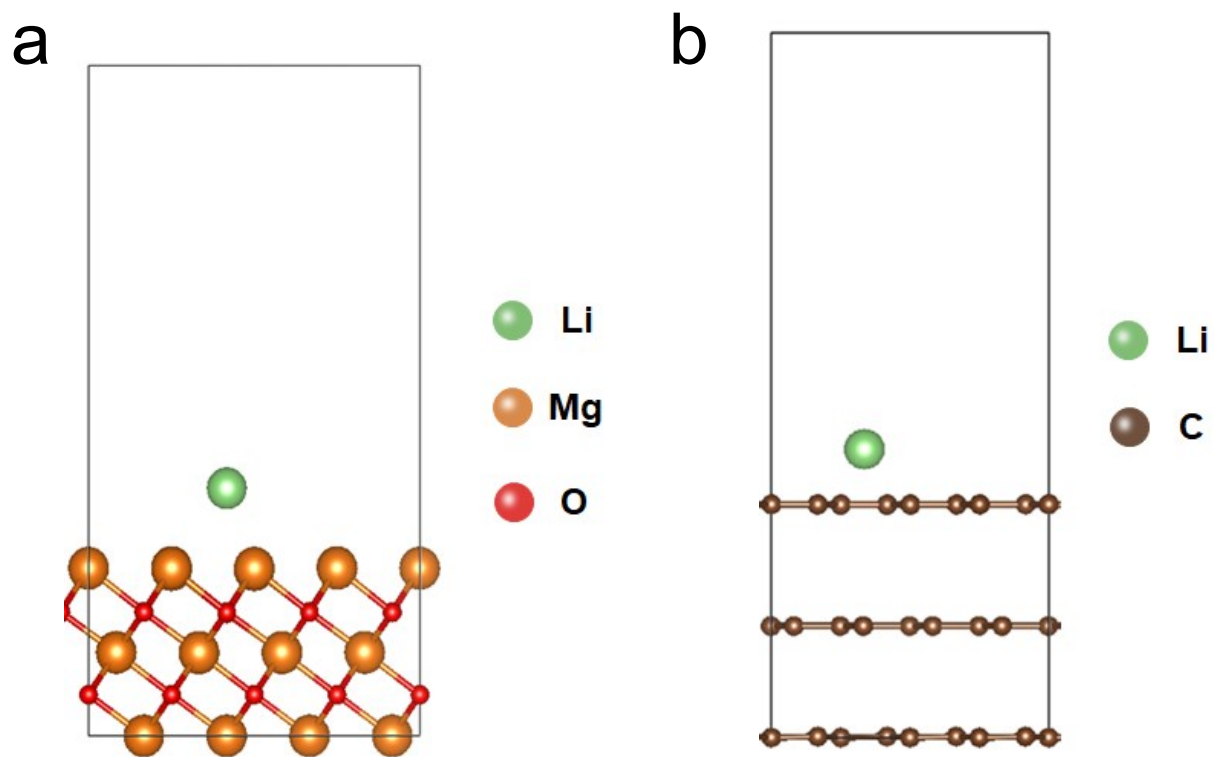


Fig. S7 The schematic diagram of the Li atom interacting with (a) MgO, (b) graphite carbon.

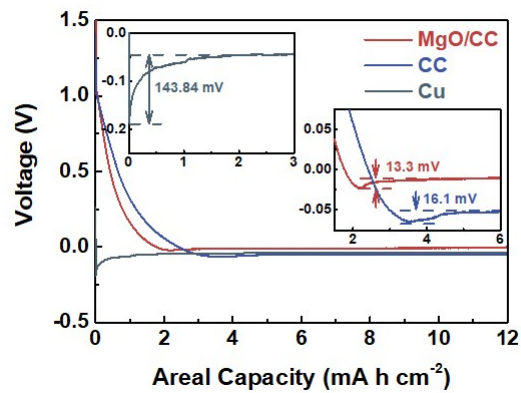


Fig. S8 The galvanostatic discharge profiles of MgO/CC, CC and Cu foil electrodes at 0.1 mA cm^{-2} in carbon-based electrolyte.

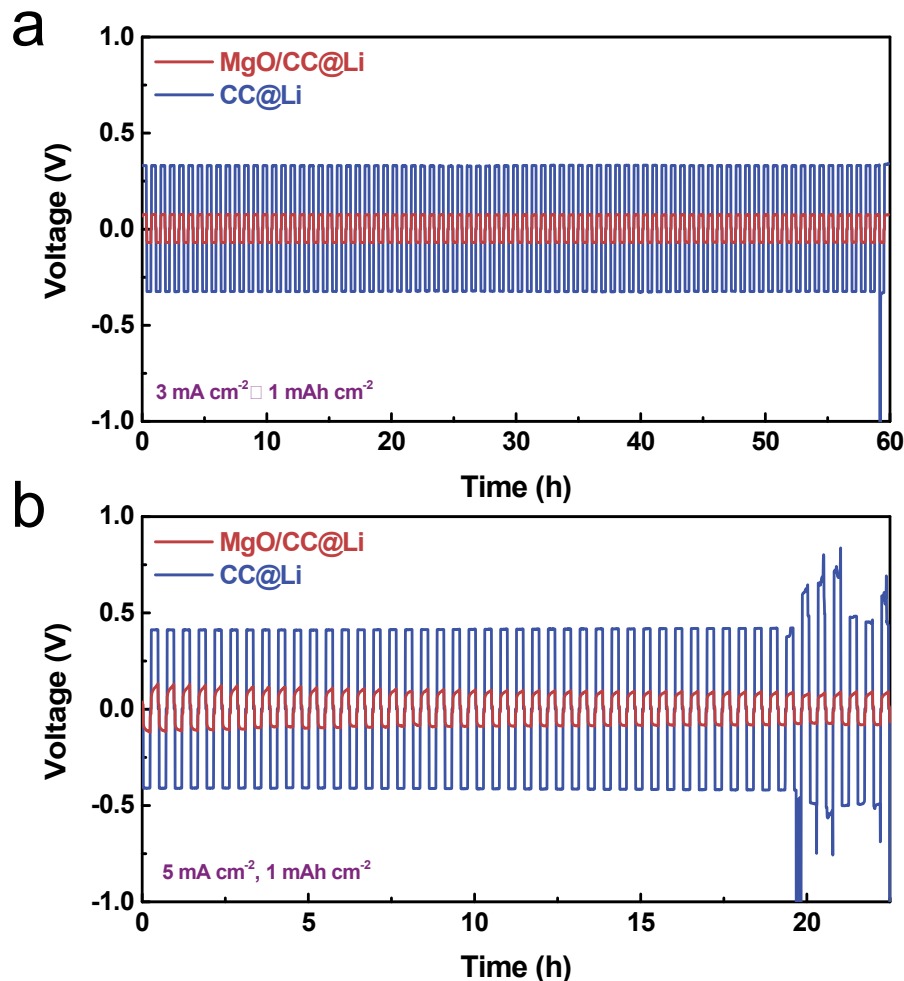


Fig. S9 Galvanostatic discharging/charging voltage profiles of MgO/CC@Li and CC@Li in symmetric coin cells at (a) 3 mA cm^{-2} and (b) 5 mA cm^{-2} with a stripping/plating capacity of 1 mA h cm^{-2} .

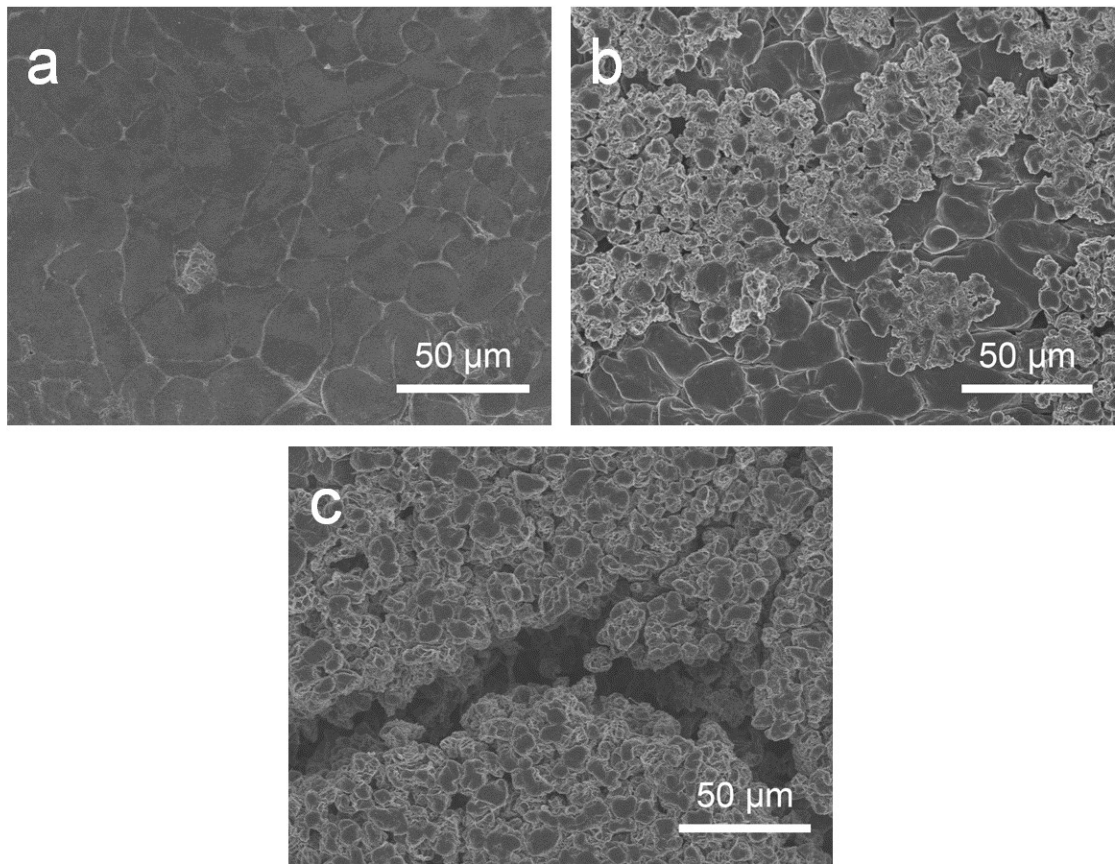


Fig. S10 SEM images of (a) MgO/CC@Li, (b) CC@Li and (c) Cu@Li electrodes in symmetric coin cells at 1 mA cm^{-2} with a stripping/plating capacity of 1 mA h cm^{-2} after 20 cycles.

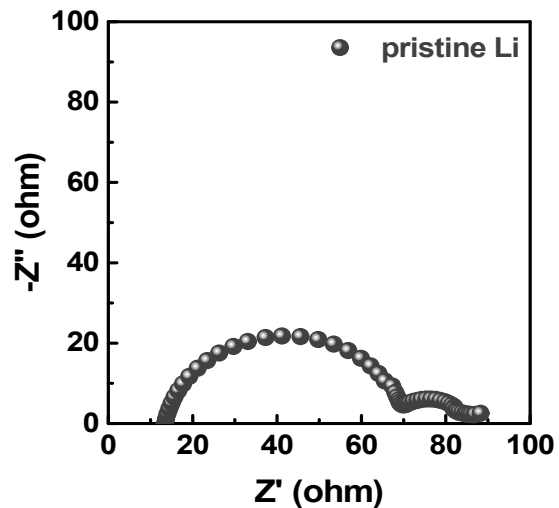


Fig. S11 Nyquist plot of the symmetric cells of two pristine Li disks.

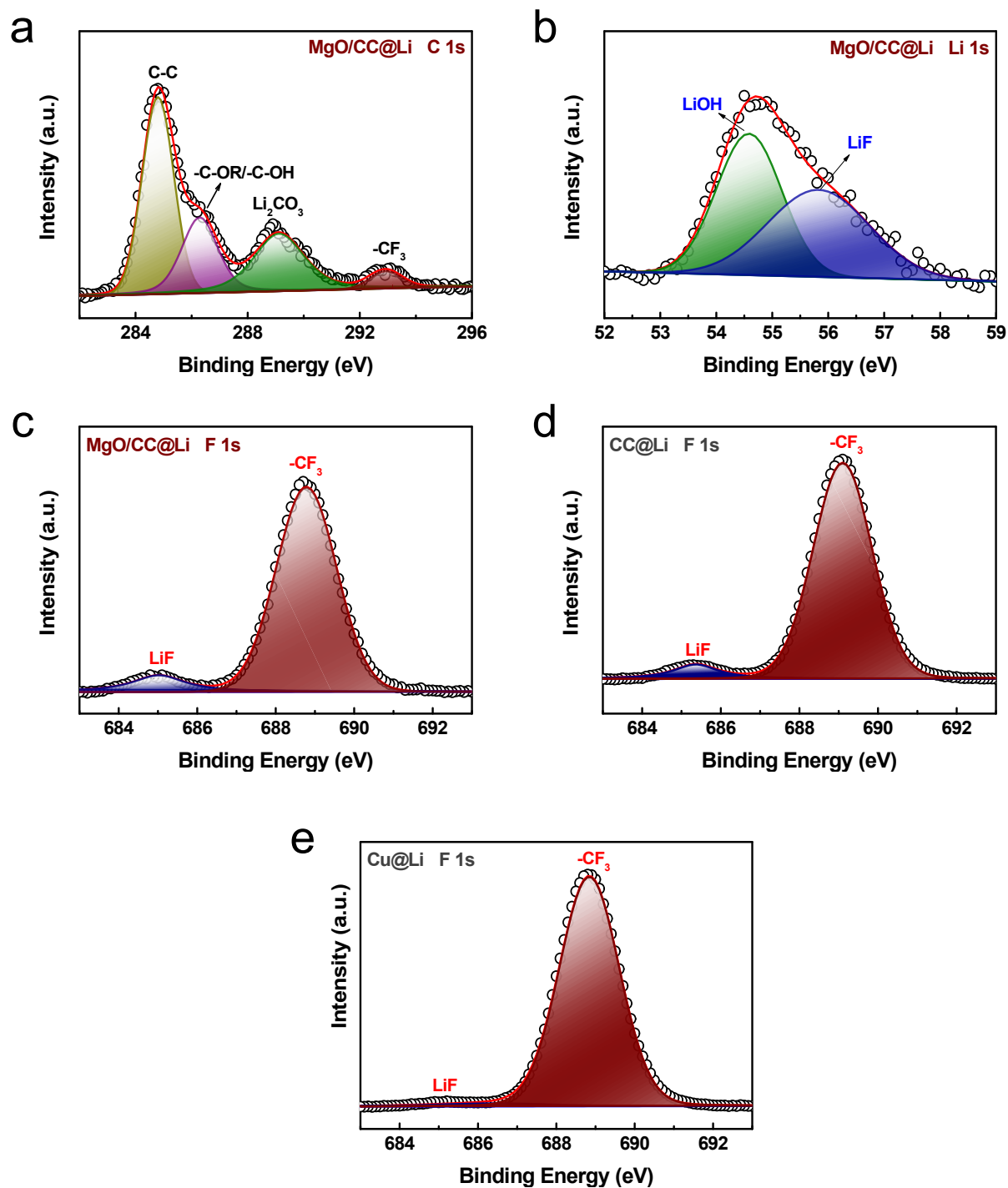


Fig. S12 XPS spectra of (a) C 1s, (b) Li 1s and (c) F 1s on the surface of MgO/CC@Li; F 1s spectra on the surface of (d) CC@Li and (e) Cu@Li anodes after 5 cycles.

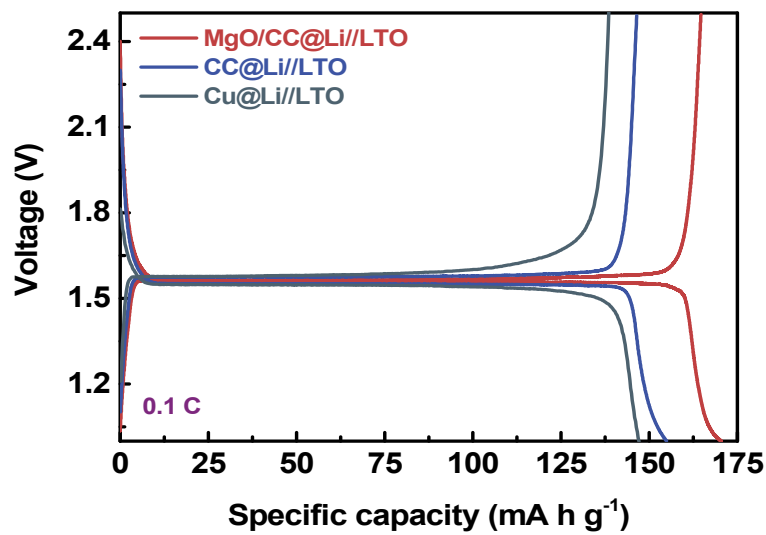


Fig. S13 Typical galvanostatic profiles of MgO/CC@Li//LTO, CC@Li//LTO and Cu@Li//LTO full cells at 0.1 C.

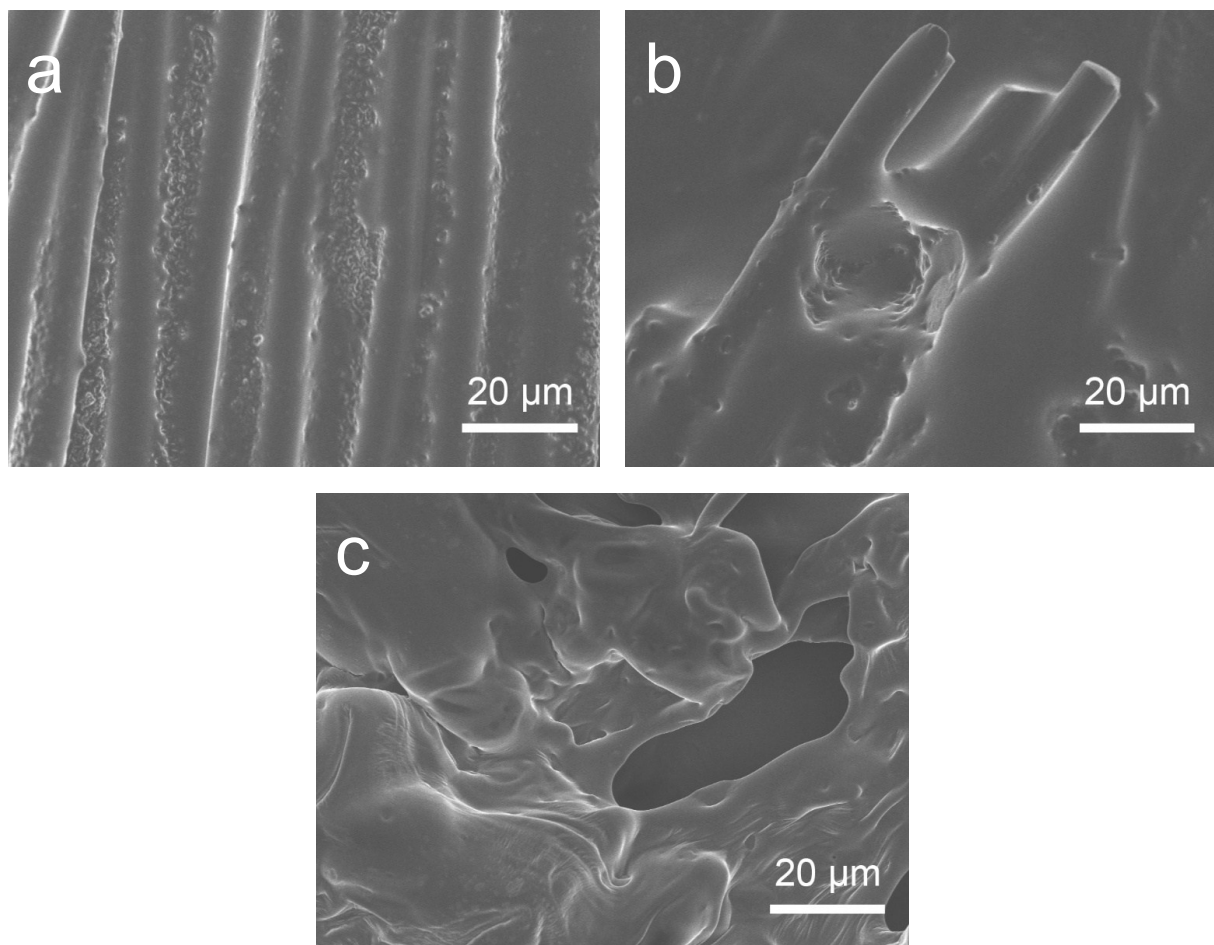


Fig. S14 SEM images of (a) MgO/CC@Li, (b) CC@Li and (c) Cu@Li anodes in full cells

after 300 cycles at 1 C.

SEM was used to further check the morphology change of the three anodes paired with LTO after 300 cycles at 1 C (**Fig. S14**). For the MgO/CC@Li anode, the Li metal deposits compactly without obvious dendrite (**Figure S14a**). In contrast, large cracks (**Fig. S14b**) and much more dendrites (**Fig. S14c**) arising from the irreversible parasitic reactions are observed on the surface of CC@Li and Cu@Li anodes. The uncontrollable growth of dendrite plus accumulation of loose inactive layer lead to the increased internal resistance and rapid capacity decay of the full cells. These results further reveal that the MgO/CC@Li anode exhibits good superiority with better mitigating effect on dendrite than other counterparts.”.

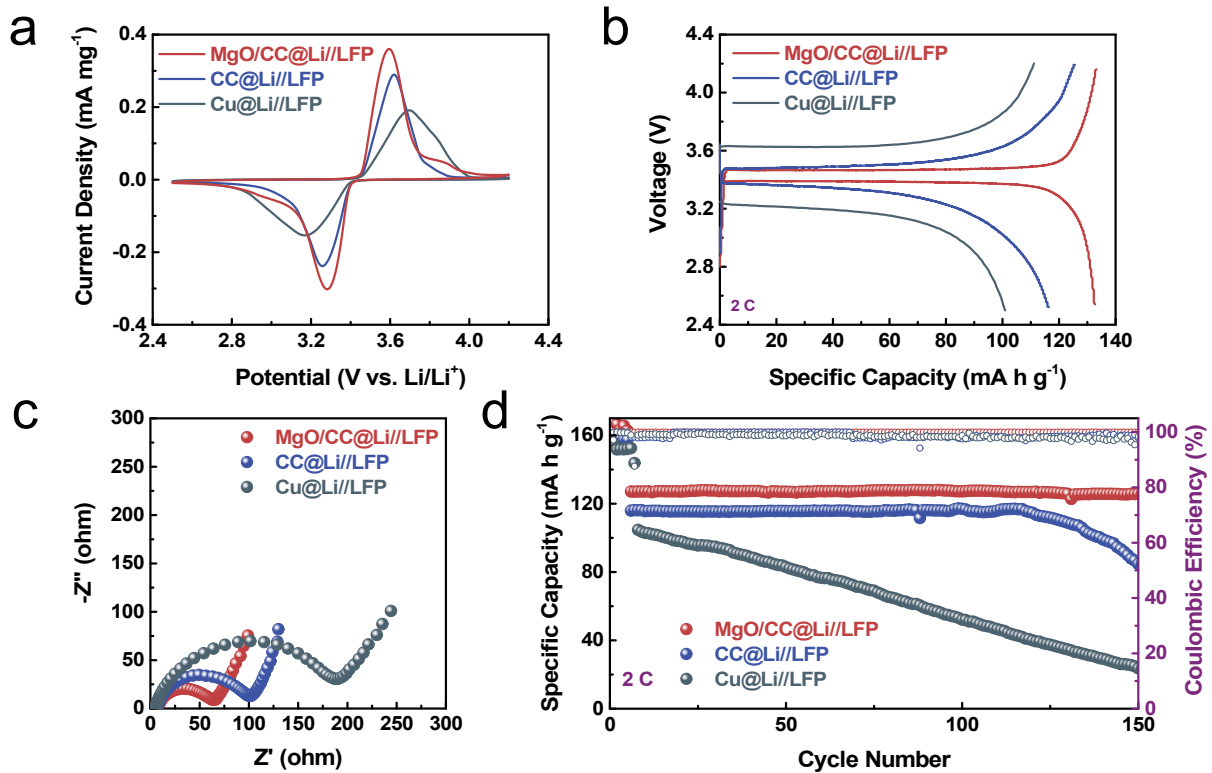


Fig. S15 Electrochemical performances of MgO/CC@Li//LFP, CC@Li//LFP and Cu@Li//LFP full cells. (a) CV curves at a scan rate of 0.1 mV s^{-1} ; (b) Typical galvanostatic profiles at 2 C; (c) Nyquist plots; (d) Cycle performance at a current density of 2 C.

To further verify the generality towards cathode materials of MgO/CC@Li electrodes, lithium iron phosphate (LFP) of 4 mg cm^{-2} was used to assemble full cells. **Fig S15a** shows the CV curves of all samples. It can be seen that the MgO/CC@Li//LFP full cells have lower oxidation potential and higher reduction potential compared with CC@Li//LFP and Cu@Li//LFP full cells, indicating that the MgO/CC@Li anodes shows better electrochemical reaction kinetics. The EIS tests were measured to evaluate the interfacial stability (**Fig S15c**). The interfacial resistance of the cells with MgO/CC@Li anodes is much lower than those of other counterparts, implying that the unique nanostructure of MgO/CC@Li anodes with enlarged surface area and lithiophilic nature can lower the interfacial resistance between the

electrode and electrolyte, which is also consistent with the lowest voltage overpotential shown in the typical galvanostatic discharge/charge voltage profiles (**Fig S15b**). For Cu@Li//LFP full cells, the capacity decays rapidly and after about 100 cycles, the capacity of CC@Li//LFP full cells also starts to decrease (**Fig S15d**). On the contrary, the MgO/CC@Li//LFP full cells exhibit an excellent cycling performance at 2 C for 150 cycles with a capacity retention of over 97 % and stable CE up to 99.8%.

Table. S2 Comparison of various anode substrates.

Current collector	Areal capacity (mA h cm ⁻²)	Current density (mA cm ⁻²)	Cycling performance
Carbon nanosphere layer ¹	1	0.25-1	more than 150 cycles at 0.25 mA cm ⁻²
Porous Cu current collector with vertically aligned microchannels (VAMCs) ²	3	1-3	20 mV for 200 cycles at 1 mA cm ⁻²
Hollow carbon shell with Au NPs ³	1	0.5	more than 300 cycles at 0.5 mA cm ⁻²
Unstacked graphene framework ⁴	5	2	150 mV for 800 h at 2 mA cm ⁻²
Graphited carbon fibers ⁵	8	0.5-2	100 mV for over 300 h at 2 mA cm ⁻²
Co ₃ O ₄ nanofiber–carbon sheet (CS) ⁶	3	1-20	50 mV for more than 800 h at 1 mA cm ⁻²
Ag nanoparticles (AgNPs) on carbon nanofibers (CNFs) ⁷	2	0.5	25 mV for 500 h at 0.5 mA cm ⁻²
MgO nanoparticles in a balsa wood derived porous carbon matrix (MgO@WC) ⁸	3.5	1.5-15	350 cycles at 1.5 mA cm ⁻²
ZnO layer on the carbon fiber cloth (ZnO/CFC) ⁹	10	0.5-5	45 mV for 200 cycles at 0.5 mA cm ⁻²
Al ₂ O ₃ -based inorganic framework ¹⁰	/	1-8	below 50 mV for 900 h at 1 mA cm ⁻²
This work	12	0.5-5	30 mV for more than 2000 h (500 cycles) at 0.5 mA cm ⁻²

Table. S3 Comparisons of overall performance of MgO/CC@Li, CC@Li and CC@Li electrodes for full cells with LTO as cathode.

Electrode	Initial capacity (mA h g ⁻¹)	Rate performance (mA h g ⁻¹)						
		0.1 C	0.5 C	1 C	5 C	10 C	20 C	0.1 C
MgO/CC@Li	157.8	164.3	155.8	149.5	122.3	114.3	111.4	156.1
CC@Li	154.9	153.0	148.2	142.9	114.4	104.7	90.5	154.3
Cu@Li	150	135.8	131.5	127	92.3	77.9	55.7	135.2

References

1. G. Zheng, S. W. Lee, Z. Liang, H.-W. Lee, K. Yan, H. Yao, H. Wang, W. Li, S. Chu and Y. Cui, *Nat. Nanotechnol.*, 2014, **9**, 618.
2. S. H. Wang, Y. X. Yin, T. T. Zuo, W. Dong, J. Y. Li, J. L. Shi, C. H. Zhang, N. W. Li, C. J. Li and Y. G. Guo, *Adv. Mater.* , 2017, **29**, 1703729.
3. Y. Liu, D. Lin, Z. Liang, J. Zhao, K. Yan and Y. Cui, *Nat. Commun.*, 2016, **7**, 10992.
4. R. Zhang, X. B. Cheng, C. Z. Zhao, H. J. Peng, J. L. Shi, J. Q. Huang, J. Wang, F. Wei and Q. Zhang, *Adv. Mater.* , 2016, **28**, 2155-2162.
5. T.-T. Zuo, X.-W. Wu, C.-P. Yang, Y.-X. Yin, H. Ye, N.-W. Li and Y.-G. Guo, *Adv. Mater.* , 2017, **29**, 1700389.
6. S. Li, Q. Liu, J. Zhou, T. Pan, L. Gao, W. Zhang, L. Fan and Y. Lu, *Adv. Funct. Mater.* , 2019, **29**, 1808847.
7. C. Yang, Y. Yao, S. He, H. Xie, E. Hitz and L. Hu, *Adv. Mater.* , 2017, **29**, 1702714.
8. C. Jin, O. Sheng, Y. Lu, J. Luo, H. Yuan, W. Zhang, H. Huang, Y. Gan, Y. Xia, C. Liang, J. Zhang and X. Tao, *Nano Energy*, 2018, **45**, 203-209.
9. S. Liu, X. Xia, Z. Yao, J. Wu, L. Zhang, S. Deng, C. Zhou, S. Shen, X. Wang and J. Tu, *Small Methods*, 2018, **2**, 1800035.
10. L. Fan, S. Y. Li, L. Liu, W. D. Zhang, L. N. Gao, Y. Fu, F. Chen, J. Li, H. L. L. Zhuang and Y. Y. Lu, *Adv. Energy Mater.*, 2018, **8**, 8.